Optical true time delay for phased-array antennas: demonstration of a quadratic White cell

Betty Lise Anderson and Craig D. Liddle

We have demonstrated a proof-of-concept optical device that can produce true time delays for a phased-array radar. This device combines White cells of differing lengths with a spatial light modulator to select between the paths on multiple bounces of a given beam. The approach can handle thousands of light beams and produce hundreds of different delays. The number of delays is proportional to the square of the number of bounces. © 2002 Optical Society of America

OCIS codes: 230.6120, 160.3710, 070.1170.

1. Introduction

Large phased-array antennas can contain hundreds of antenna elements, but to steer the radar beam requires independently controllable time delays for each antenna in the array. Phase shifting works well only for a single frequency; true time delays (TTDs) are required for broadband antennas.[1] The delays required may vary from picoseconds to hundreds of nanoseconds, depending on the bandwidth of the antenna and the required steering resolution. Implementing these time delays electronically, however, is unappealing because of the long lengths of coaxial cable or strip line required and the concomitant weight and cost.

Optical approaches are more attractive. In optical TTD, the signal from (or to) each antenna element is intensity modulated onto a separate light beam, and each light beam is directed through paths of varying lengths to introduce relative time delays. These paths can be in fibers or waveguides[2–17] or in free space.[18–21] Most approaches use fibers or waveguides. Free-space approaches generally have lower loss, but beam divergence over long optical paths can create a need for physically large components, particularly switches. This problem is compounded when many beams must be simultaneously controlled as in large phased-array radars.

Our approach falls in the free-space category but is designed to avoid the divergence problem. It is based on the White cell,[22] an arrangement of three spherical mirrors that produces a multiple-bounce pattern for a given input beam. It has the added feature of refocusing the beam to a new spot on each pass. In a previous paper[23] we proposed several optical TTD devices, in which we adapted the White cell to TTD by replacing one of the mirrors with a spatial light modulator (SLM) and then using the SLM to control the number of times the light beams bounced and thus the time delay. In that linear demonstration, the number of delays was proportional to the number of bounces.

In this paper we report on the demonstration of a quadratic time-delay cell, in which the number of delays that can be obtained is proportional to the square of the number of times a beam passes through the White cell. It should be noted that the greater the number of different delays, the greater is the number of directions in which the radar beam can be steered, an important figure of merit. The number of bounces a given beam can make in the TTD device is limited by the space–bandwidth product of the SLM (related to the number of pixels), as well as the loss. The loss is expected to be the limiting factor.

A second figure of merit for TTD devices is the number of light beams (and thus antenna elements) that can be controlled simultaneously. More beams means a larger array and better (radar) beam shaping. In the case of the White cell approach, the number of beams is limited by the number of available pixels of the SLM.

An ideal TTD device would have both a large num-

B. L. Anderson (anderson@ee.eng.ohio-state.edu) is with the Department of Electrical Engineering, Ohio State University, 205 Dreese Laboratory, 2015 Neil Avenue, Columbus, Ohio 43210. C. D. Liddle is with JDS Uniphase, 2727 Scioto Parkway, Columbus, Ohio 43221.

Received 15 October 2001; revised manuscript received 15 April 2002.

0003-6935/02/234912-10$15.00/0

ber of light beams and a large number of different delays attainable. Such goals are achievable for high-space–bandwidth-product SLMs such as microelectromechanical (MEM) micromirror arrays, which may have millions of pixels. Such a MEM device has been in use by Texas Instruments for display applications for several years. Because MEM devices designed for optical switching applications (as opposed to displays) are not yet widely available, particularly not yet with large pixel count, we demonstrated our approach experimentally using a liquid-crystal SLM. For a truly large time-delay device, supporting thousands of beams and thousands of delays, a MEM device will provide lower loss, lower cross talk, insensitivity to polarization, and higher reliability.

We begin our discussion of the White cell approach to optical TTD by briefly reviewing the White cell (more detailed discussions can be found in Refs. 22 and 23). Then we show how to adapt the White cell to TTDs. In Section 3 we discuss the design process, and in Section 4 we describe the experimental apparatus. Section 5 contains experimental measurements, and in Section 6 we provide a summary and conclusions.

2. White Cell and Its Use in Time Delays

A. White Cell

The optical TTD device we describe is based on the White cell, the operation of which we review briefly here. The White cell was developed in the 1940s for optical spectroscopy, in which long paths through weakly absorbing gases were required.[22,24] The White cell consists of three spherical mirrors, all having the same radius of curvature, arranged as shown in Fig. 1(a). The mirror on the right (A) has its center of curvature CC(A) located in the plane of the other two mirrors, B and C, between those two mirrors. The centers of curvature of mirrors B and C are located on the surface of mirror A, as shown in Fig. 1(b), and are separated by a distance δ.

A beam is introduced into the cell as a spot on an input turning mirror in the plane of mirror A. The light is directed to mirror B and will in general diverge. Mirror B images the input spot to a new spot on mirror A, located on the opposite side and an equal distance from Bs center of curvature [labeled CC(B)]. We call that image spot the first bounce.

Mirror A, however, images light from mirror B onto mirror C. This is a nice feature of the White cell because all the light from B necessarily appears on C, and thus no light is lost to diffraction or truncation. Thus the light goes next to mirror C.

Meanwhile, spot 1 is an object for mirror C and is refocused to a new image back on mirror A on the opposite side of CC(C). This is bounce two. Mirror A again images the light returning from mirror C back onto mirror B.

This process continues, forming a set of spots on mirror A as indicated in Fig. 1(b). In general a given input beam generates a spot pattern in two rows. The number of spots or bounces is determined by the tilts of mirrors B and C—that is, where their centers of curvature are located, along with the overall size of mirror A.

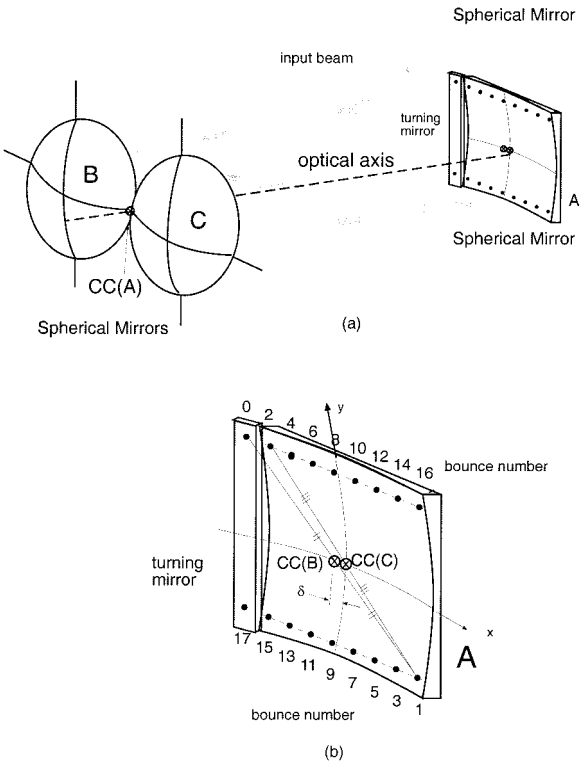

Fig. 1. (a) White cell consists of three spherical mirrors all of the same radius of curvature. A spot enters the cell through an input turning mirror. (b) The White cell produces a spot pattern on mirror A. Mirror B images the input spot to spot 1, and mirror C images spot 1 to spot 2. Even spot numbers increase to the right, and odd spot numbers increase to the left.

Recalling that we will need a separate light beam for each antenna element, we look for ways to introduce more beams. One solution is shown in Fig. 2(a). Here the three different shapes represent three different light beams. Each traces out a unique spot pattern on mirror A. In Subsection 2.B we replace this mirror with a SLM, so the reader will anticipate that these spots will be mapped to pixels and that each light beam can be controlled on each bounce. In fact, depending on the separation between the spots in a given row, it is possible to also circulate multiple beams in each row as can be seen in Fig. 2(b). Here the bounce pattern for 33 input spots (in three columns and 11 rows) is shown. Each of the 33 input beams strikes a unique set of places on mirror A.

B. Adapting the White Cell to Time Delay

In a traditional White cell, a beam bounces a given number of times in the cell and thus experiences a fixed time delay. To change the delay time, we fix the number of bounces, but we switch between paths of different lengths on each bounce. As foreshadowed above, to do the switching we replace spherical mirror A with a (flat) SLM to reflect the light and add

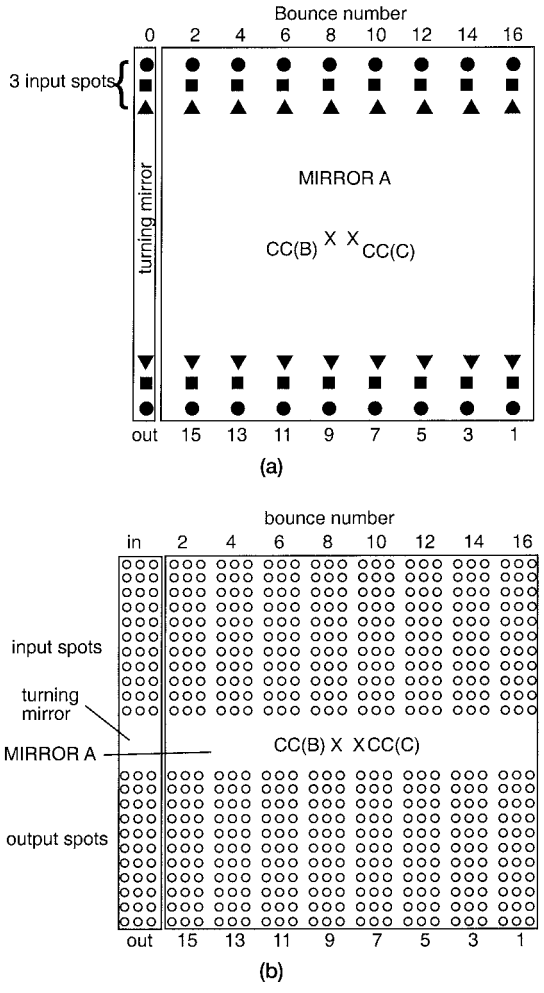

Fig. 2. (a) Additional beams can be introduced into the White cell, and each traces a unique spot pattern. (b) The input beams can enter in an array, but each beam still strikes a unique set of spots.

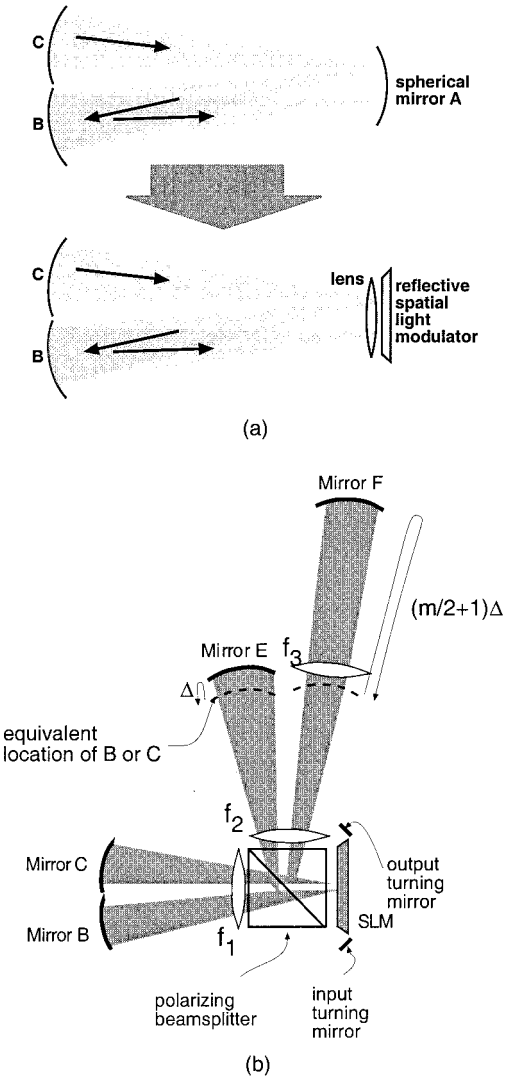

Fig. 3. To implement switching, we modified the White cell (a) by replacing mirror A with a liquid-crystal SLM and a lens (f_1) to create a White cell in which the polarization can be switched on any bounce for any beam. (b) To form the quadratic cell, a polarizing beam splitter is added to direct the light to alternate White cell mirrors E and F. The distances to E and F are different than to B and C, thus introducing time delays.

a lens to provide the focusing property of the curved mirror This is shown in Fig. 3(a). Optically such an arrangement is still a White cell.

Let us take the SLM to be a reflective liquid-crystal type. We align the device such that each spot lands on a unique pixel. Then the polarization of each beam can be changed on each bounce. We add a polarizing beams splitter (PBS) to direct the beam into different paths based on its current polarization state.

Next, to make alternate paths of different lengths, we add a second pair of White cell mirrors as shown in Fig. 3(b). A second White cell consists of mirrors E and F and the SLM–lens combination. We also added another lens to the arm containing mirror F, which we discuss below. In this case the White cell mirrors (E and F) have different radii of curvature, but their centers of curvature are both still located on the SLM. (Technically it is the images of their centers of curvature, through lens f_2, that are on the SLM.) The (image of) the center of curvature of mirror E is superimposed on that of mirror B, and the center of curvature of mirror F is superimposed on that of mirror C. The lens f_3 is required because a single lens f_2 cannot place the center of curvature images of both E and F on the same plane. With the centers of curvature of the corresponding White cell mirrors superimposed, a beam will trace the same spot pattern on mirror A, regardless of whether its path is BCBC . . . , EFEF . . . , BFEC . . . .

Next let us consider the distances. The transit time for a beam to go from the SLM to mirror E and back to the SLM (one round trip) is longer than the transit time to B or C by some time increment Δ. The round-trip time through mirror F is longer yet by some amount to be chosen, as we show below. The operation of the TTD cell is as follows.

The number of bounces is fixed at some number m. If the SLM is addressed such that a given beam's

polarization is never changed, the light travels in the path SLM–B–SLM–C–SLM–B . . . . This is the shortest path that a beam can travel, and the time it takes to do it m times is common to all beams. This time bias affects all antenna elements equally and does not contribute to antenna steering; it is, in effect, subtracted out. We call this a delay of zero.

If, however, the polarization is switched on a given bounce, the beam is directed into the EF White cell. The beam can visit either mirror E or F depending on whether this happens to be an even- or odd-numbered bounce. Suppose the light is sent to mirror E, and that on the following bounce the polarization is switched back. Then after 20 bounces, the beam will have gone to mirror E one time and incurred a delay of Δ relative to a beam that goes only to B and C. The beam can be sent to mirror E only on every other bounce or at most $m/2$ times. Thus delays up to $(m/2)\Delta$ can be obtained with mirror E. Actually, it is one less than this, $(m/2 - 1)\Delta$, because the light is constrained to go to mirror B first from the input turning mirror.

Let us now suppose that the arm containing mirror F is made longer than B or C by one more than the maximum $(m/2 - 1)\Delta$ or $(m/2)\Delta$. The beam can visit F at most $m/2$ times as well. We therefore obtain the maximum delay by visiting mirror E for a delay of Δ at every opportunity ($m/2 - 1$ times) and mirror F at every opportunity ($m/2$ times) for a delay of $(m/2)\Delta$ each time. The total number of possible different delays N is then

$$N = \left[\left(\frac{m}{2}\right)\left(\frac{m}{2}\right) + \left(\frac{m}{2} - 1\right)\right] = \left[\left(\frac{m}{2}\right)^2 + \left(\frac{m}{2}\right) - 1\right]. \quad (1)$$

Any integer delay from 0 to N can be obtained with the proper combination of trips to mirrors B, C, E, and F.

We call this cell quadratic because the number of delays obtainable is proportional to the square of the number of bounces. This distinguishes this design from other linear designs discussed in Ref. 23.

It should be emphasized that the size of the time-delay increment Δ can be arbitrarily small—the delay is the difference between two paths, not the length of any particular path. Thus long and short delays are equally easy to implement with this design.

3. Design of the Quadratic True Time-Delay Device

In this section we discuss our actual design and the process used to obtain it. First, we folded the longest White cell arm (the one containing mirror F) as shown in Fig. 4. Here we replaced lens f_3 with a spherical mirror F′. Second, we added one additional lens f_4. This lens is placed at a plane conjugate to the SLM, so the spot pattern from the SLM is reproduced at this plane. In this way, we can move the input and output turning mirror to this image plane rather than have it next to the SLM as it was in Fig. 3. This modification was advantageous from a fixturing point of view because the turning mirror must be in the plane of the spots, and the SLM housing is in practice too bulky to allow this. Finally, we folded the path of the longest arm again using a flat mirror.

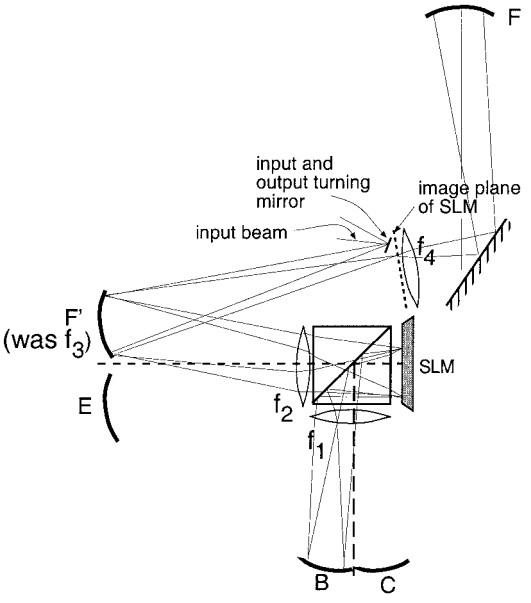

Fig. 4. In our apparatus, the longest path is folded for compactness, and a new image plane of the SLM is introduced to facilitate inputting the beams.

We chose a 1-ns time-delay increment of $\Delta = 1$ ns. This means that the round-trip path to mirror E from the SLM should be 300 mm longer than the path to B or C. To set the distance to F we must fix the number of bounces m, which was chosen to be ten. Thus the path to F (through F′ and lens f_3) should be $(m/2 + 1)\Delta$ or 6 ns (1.8 m) longer than the null path.

There are several imaging conditions that must be satisfied for the device to operate as a White cell:

1. The SLM must be imaged on itself by mirror B. It must almost image onto itself through each of the C, E, and the F′–f_4–F routes.
2. Mirror B must image onto mirror C through the SLM.
3. Mirror E must image onto mirror F through the SLM (and F′ and f_4).
4. Mirror B must image onto mirror F through the SLM (and F′ and f_4).
5. Mirror C must image onto mirror E through the SLM.
6. The SLM images onto lens f_4 to produce a spot pattern there. (This last condition is not required but was a design choice.)

Figure 5 shows the first and second conditions. In Fig. 5(a) the SLM images onto itself through one of the White cell mirrors (for example, B), and Fig. 5(b) shows B imaging onto C through the SLM.

Using these six imaging conditions, we can design the cell. For example, the second condition requires that the separation d_B between mirror B and lens f_1

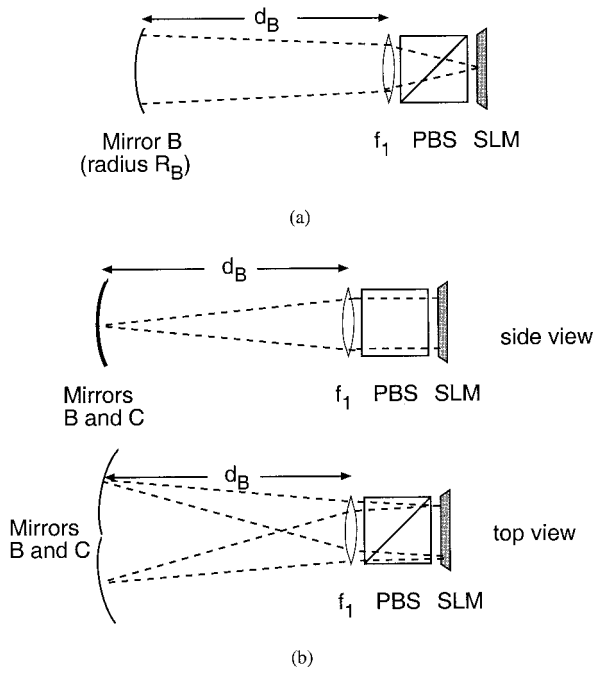

Fig. 5. Two main imaging conditions in a White cell are that (a) the SLM must image onto itself through each of the White cell mirrors (B is shown), and (b) each White cell mirror must image back onto each of two other White cell mirrors through the SLM. The case for B imaging on C is shown. B and C are in the same plane.

should be equal to the focal length f_1. By choosing the size of the PBS and knowing its refractive index, allowing a little distance d_{SLM} between the PBS and the SLM for fixturing ease, and choosing a standard catalog lens f_1, we can choose a reasonable radius of curvature for mirror B. We followed this process using ray matrices and thin-lens approximations. Once the radius of B was found, a standard catalog value close to that was chosen and the distances adjusted to maintain the imaging conditions. The arm containing mirror C is identical to that of mirror B. Recall that the overall length of the B–C White cell is arbitrary and does not contribute to the time delays.

A similar procedure can be used to design the arm containing mirror E; however, there is the additional constraint of requiring the total length of arm E to be 150 mm (half of a 1-ns round-trip time) longer than the total length of arm B.

The folded arm containing mirror F is also straightforward to design. Mirror F′ can be chosen the same as mirror E and placed in that same plane. The image of the SLM appears at lens f_4, and mirror F is conjugate to mirror F′. In Fig. 4 the magnification of the SLM image would be -1. However, we modified this arrangement as shown in Fig. 6. We demagnified the SLM image somewhat, which reduces the required size of lens f_4 and allows the lens to be moved closer to the main axis of the device. This means that the angle of the fold is reduced, thus decreasing the astigmatism. This design change places mirror F′ a little behind the plane of mirror E. Then the combination of lens f_4 and mirror F is chosen to satisfy the remaining imaging conditions (3 and 4) as well as the requirement that this path is 6 ns longer than the path with mirror B or C. It is still the case that the SLM is conjugate to the input plane (containing lens f_4) and that mirror F′ is conjugate to mirror F. Figure 6 gives all the final design distances, lens focal lengths, and mirror radii of curvature.

A ray trace is also shown in Fig. 6. The solid lines represent a spot on the lower edge of the MEM array being reimaged to a new spot near the top. Note that the same new spots reform whether the light goes to mirror C or to mirror F. From there, the dotted lines shown the rays going to the next image, which is the same whether the light goes to B or E.

4. Experimental Apparatus

Here we describe an experimental apparatus and present our time-delay data, along with loss and cross talk.

The input source for our experimental apparatus was a diode-pumped Nd:YAG laser emitting at 1319 nm, as shown in Fig. 7. The laser has a polarization-maintaining fiber output that was coupled to a Mach–Zehnder intensity modulator to modulate the rf signal onto the beam. We then divided the modulated optical signal using a 1×8 power fiber splitter (also polarization maintaining). Four of these outputs were connected to the input leads of a 1×4 fiber V-groove array. The other four outputs were diverted to another experiment. The fibers in the V-groove array had a pitch of 250 μm, matching the pixel pitch of the SLM. The SLM was a 256-element liquid-crystal SLM.

The time-delay part of the apparatus is shown in the lower part of Fig. 7. Not all the TTD cell is shown. The SLM was a 16×16 array of 100-μm-square pixels. At a 250-μm pitch, the overall image size of the SLM was 4 mm by 4 mm. The liquid-crystal material was ferroelectric, and the pixels were direct driven. The device was designed to operate at 1319 nm. The reflective backplane was gold. The front of the SLM was coated with a transparent conductor (indium tin oxide).

The fast and slow axes of the liquid crystal were parallel to the sides of the array. Because our laser light was polarized vertically, we used a half-wave plate ($\lambda/2$) to rotate our light polarization by 45° to excite both eigenpolarizations of the SLM.

The input spots from the four fibers were imaged onto the input turning mirror for introduction into the White cell. The image size was doubled, placing the input spots on a 500-μm pitch. This meant that we used every other pixel on the SLM, but we also doubled the spot size to approximately 20 μm. This was done to lower the power per area and avoid damaging the SLM.

For input and output, we used a power-dividing beam splitter to direct the returning light to a high-speed photodetector (diameter of 25 μm). In practice a separate output turning mirror would avoid the

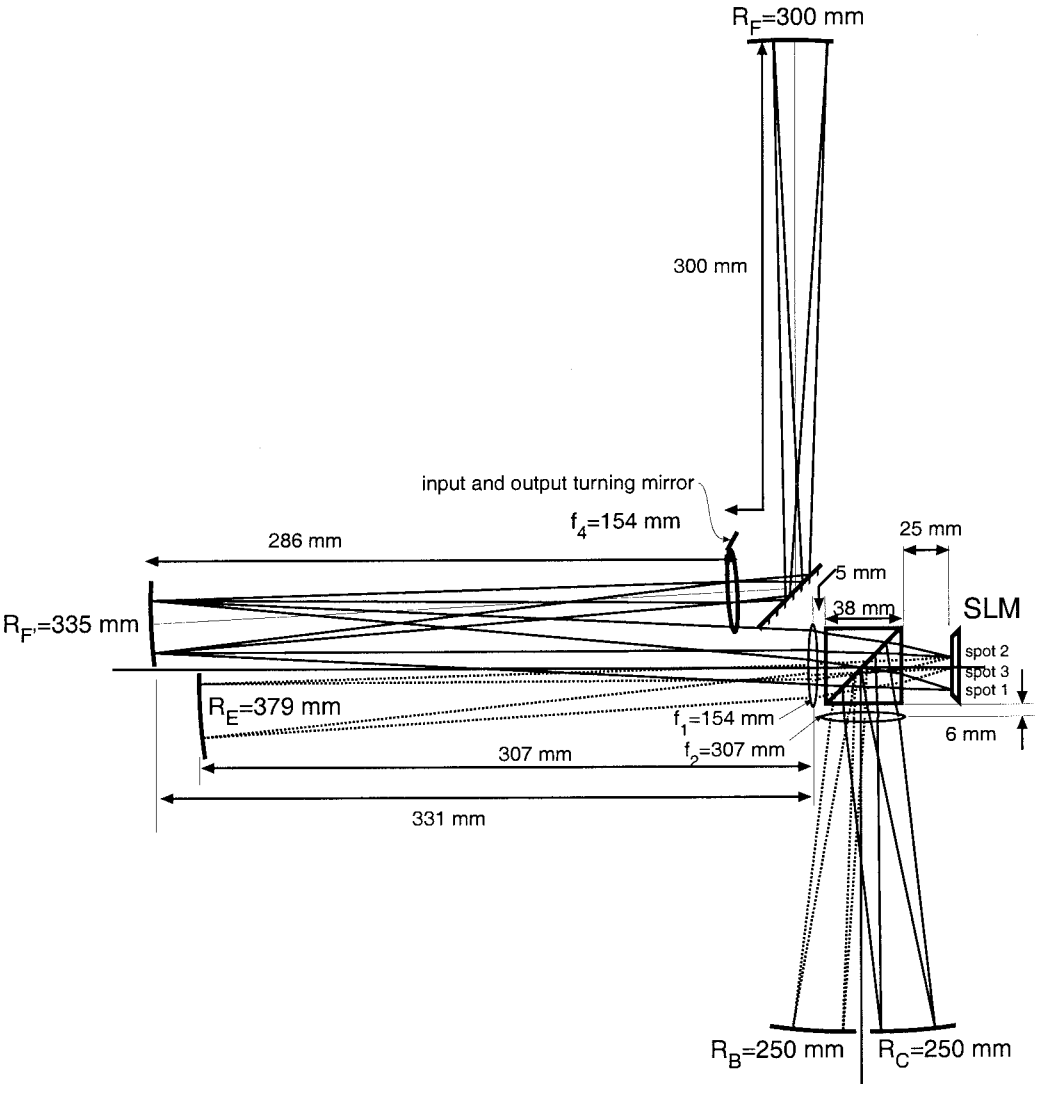

Fig. 6. Final White cell design for a time-delay increment of 1 ns. A ray trace shows how a spot from the SLM images to another spot through any of the arms B, C, E, or F. Solid lines, SLM images onto itself through either C or F; dotted lines, SLM images onto itself either through B or E.

excess loss of the beam splitter, but in our case the power level was quite high. Thus we simply reused the input path. Also, we placed a detector at only one of the four output spots to measure time delays, loss, and cross talk. A diode array would be required to measure multiple beams simultaneously.

5. Experimental Results

A. Alignment

The cell was designed to operate with ten bounces. Recall that the number of times a beam bounces in the cell is determined by the positions of the centers of curvature of the various White cell mirrors (B, C, E, and F). By adjusting these, we demonstrated up to 18 bounces before the losses became too great to observe them. Alignment in a White cell is simple because once the 18th bounce is aligned on the proper pixel, all the preceding bounces are necessarily aligned as well.

We had difficulty maintaining this alignment over long periods of time because of the low-cost spring-type mirror mounts we used. Over the course of a day these would sag and shift enough to spoil the alignment. Therefore, when measuring time delays, a process that takes some time to set up and do, we were restricted to a four-bounce pattern.

B. Time Delays

We measured the time delays using a network analyzer. The rf was swept from 2 to 12 GHz and modulated onto the input beams. Figure 8(a) shows the reference beam. In our experiment, this beam was directed such that it went back and forth between White cell arms E and F only; thus it experienced the longest possible time delay. Figure 8(b) shows the result when the beam is switched to mirror B one time (thus avoiding one trip to mirror E). This beam arrives at the output 1 ns earlier than the reference.

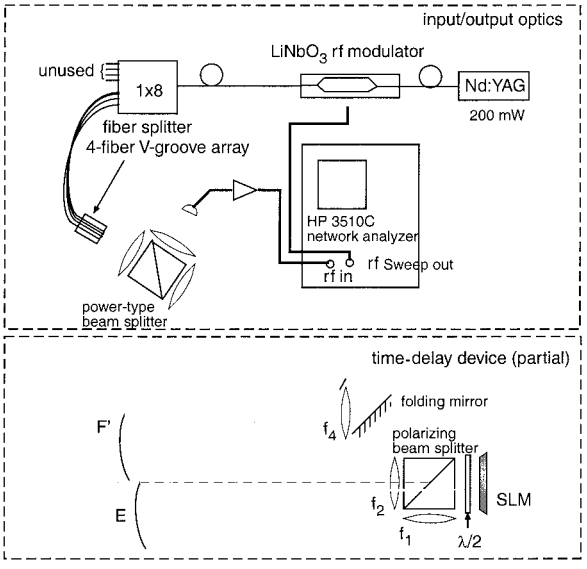

Fig. 7. Experimental input optics and measurement apparatus. Light from a 1319-nm Nd:YAG laser is modulated with a frequency-swept rf signal. The light is divided into four input beams by a fiber splitter, and the fiber output faces are imaged onto the input turning mirror. The output beams are separated with a power-dividing beam splitter and sent to rf photodetectors. The demodulated rf signals are measured with a network analyzer, and the time delays are determined.

Similarly, a beam directed to mirror C one time avoids one trip to F and thus arrives at the output 6 ns earlier. Thus all the appropriate time delays were demonstrated along with the ability to switch between them.

C. Loss

We measured the output power after each bounce and found a loss per bounce of 1.06 dB (optical, not electrical). This loss is quite high, as is to be expected from a liquid-crystal-based cell. Most of the loss, 0.6 dB, results from the SLM, the primary contribution coming from the transparent conductor (5%). A significant contributor was also the gold, at approximately 97% reflectivity at 1.3 μm. The Fresnel reflections from other layers in the SLM (such as the antireflection-coated glass) and the loss in the liquid-crystal material itself are negligible. After the SLM, the next largest contributor was the PBS, at approximately 0.25 dB/pass (we used an ordinary broadband cube beam splitter). The range of incident angles in our White cell was not large enough to make the losses vary from bounce to bounce. Each beam, however, passes through the beam splitter twice on every bounce. Thus the SLM and PBS together contribute an expected 1.1 dB/bounce; the mirrors and lenses are negligible. Clearly a better SLM is needed, the most likely candidate being MEM mirror arrays, whose loss is expected to be below 0.1 dB/bounce.

Note that the loss we encountered compares favorably to a total worst-case loss of 1.17 dB predicted from the losses at each surface. Because our worst-case prediction excluded diffraction, and because we beat the worst-case prediction, we conclude that diffraction losses are small. We emphasize that low diffraction loss is a natural result of the White cell configuration, which avoids diffraction losses by repeated imaging of one mirror to another.

In our apparatus we took the output directly from a photodetector, but in a phased-array radar the signal processing can be done remotely, requiring a fiber link. Thus there will be additional loss coupling from the White cell spots into the fiber. In this case, we can assume that the input spots also come from the fiber, and thus the fiber mode is repetitively reimaged. As long as the magnification is unity, and the spots are much less than the pixel size to avoid truncation effects, the coupling loss is not affected by passage through the White cell. We demonstrated this in the laboratory for a simple White cell (no SLM). We compared the coupling efficiency from the White cell free-space output spot to a single-mode fiber with the coupling efficiency going from a fiber to a collimated beam back into the fiber. The losses were identical to within experimental error (1.9 dB $\pm$ 0.02 dB).

Finally, we comment that the losses we measured are also impacted by the polarization cross talk, discussed in Subsection 5.D.

D. Cross Talk

There are two types of cross talk of interest in this device. One is the intraelement cross talk, which occurs when the polarization is not completely pure. (In a MEM-based device, the only intraelement cross talk would result from scattering or beam divergences larger than the MEM tilt angle.) This results in some light traveling to the wrong arm of the dual White cell, meaning that some of the light arrives at the correct antenna element of the phased-array radar but arrives at the wrong time. We measured high cross talk of this type—approximately 50%. This turned out to be because the SLM vendors generally expect the user to switch polarizations, but discard one of the beams and keep the other. Thus they provided excellent extinction (100:1) for one polarization. The other is extinguished only approximately 50%, accounting for our cross-talk results. We, on the other hand, keep and reuse both beams. Had we adequately specified our extinction requirements, the liquid crystal could have been designed for good extinction for both polarizations.

The second type of cross talk is interelement cross talk, which results when light from one pixel leaks onto a pixel belonging to the spot pattern of another light beam. In this case, some of the light arrives at the wrong output. Recall that in our setup we were using every other pixel. We interlaced the spots in such a way as to bring neighboring light beams onto adjacent pixels, and we found a cross talk of -11 dB. This resulted from the rather large feet of the input beams in our apparatus and could be reduced further by better design of the input optics.

Another consequence of the large feet that could

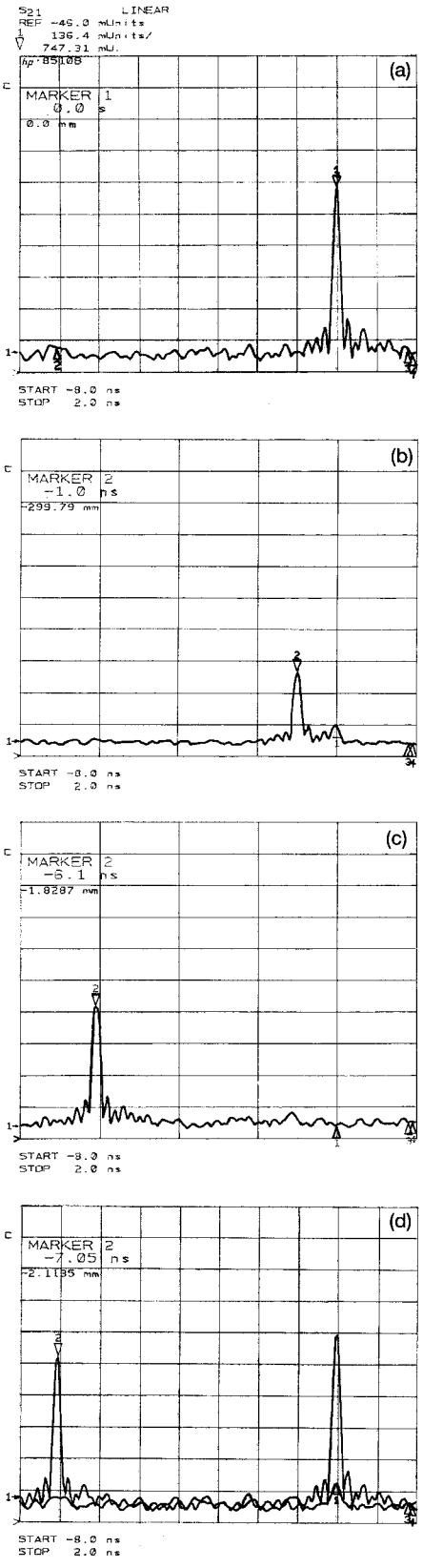

Fig. 8. Experimental time-delay data for several delays. (a) The beam goes to A and F every time, and incurs the longest delay. This is our reference delay. (b) The beam goes to E one time fewer and arrives at the output 1 ns earlier. (c) The beam goes to F one time fewer and arrives 6 ns earlier. (d) The beam goes to E and F one time fewer each and arrives at the output 7 ns earlier.

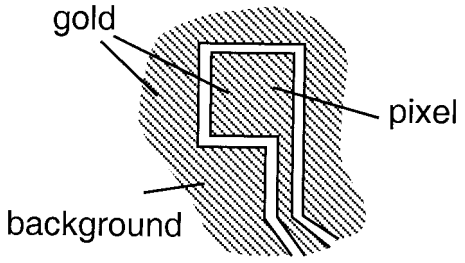

Fig. 9. Gold backplane pattern of the SLM can introduce cross talk. When a beam overlaps onto the backplane, it is reflected but in an undetermined polarization state.

potentially have contributed to both types of cross-talk results from the gold backplane of the SLM. Figure 9 shows the backplane pattern of the SLM in the neighborhood of a pixel. The feet will extend onto the backplane and be reflected back into the apparatus, but the polarization state is controlled only in the pixel area. The light from the feet is in an undetermined polarization state and can go into both White cells. If that light is not precisely reimaged on the backplane again, it can eventually leak onto a pixel and be delivered to an antenna element.

6. Discussion and Summary

We have presented the design and demonstration of a quadratic optical TTD device, for phased-array radar antennas, based on the White cell. Quadratic means that the number of delays that can be obtained is proportional to the square of the number of bounces, an improvement over our previous linear design. There is one input beam per antenna element in the array, and each beam bounces a fixed number of times in the apparatus. The device contains two White cells, and the arms of the cells are of varying lengths. A SLM is used to switch between the paths, thus varying the time it takes a given beam to transit the cell. In our experiment we used a liquid-crystal SLM because of its availability. As mentioned above, there are two criteria by which the performance of a TTD device is measured. One is the number of light beams that can be supported—at one light beam per antenna element, more beams means a larger antenna array and thus a better quality radar beam that can be delivered. The number of light beams that can be handled in a single White cell device is determined by the number of pixels available on the SLM and the number of bounces.

The other performance criterion is the number of different delays that can be provided. In the quadratic cell the number of delays obtainable is proportional to the square of the number of bounces a given beam makes in the cell. The number of bounces is set by the designer and, in practice, will be limited by the tolerable loss. If there are M light beams each making m bounces, then the number of pixels required is $M \times m$. A 256×256 element SLM would support 3276 beams making 20 bounces each, or a 3276-element phased-array radar with 109 different delays.

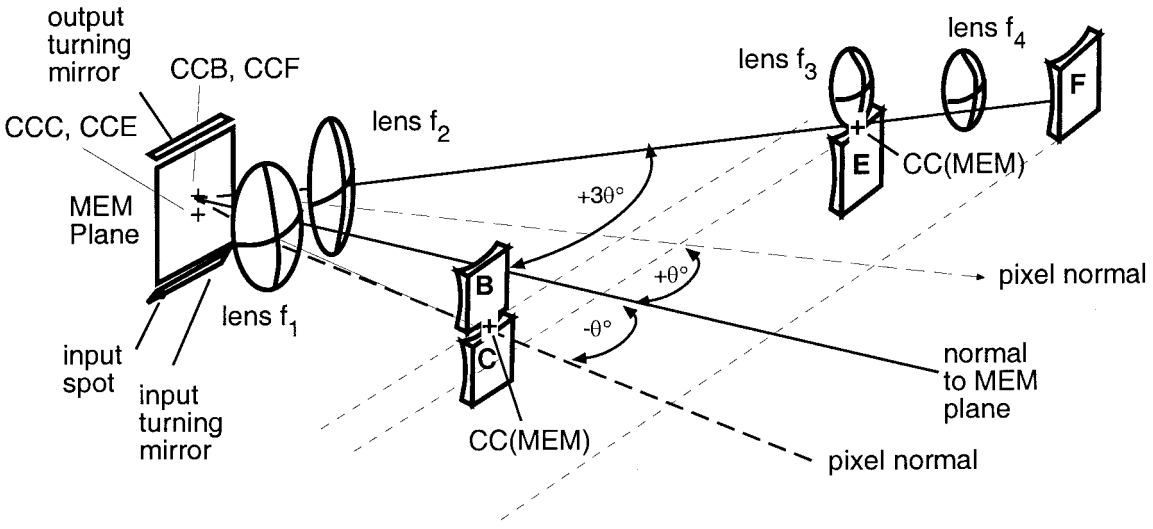

Fig. 10. One design for a MEM-based quadratic optical TTD device. The MEM micromirrors are assumed to be able to tip to one of two stable positions at $\pm\theta$. One White cell is formed along the -θ (mirrors B and C), and two more spherical mirrors are placed along the $+3\theta$ axis.

Arrays typically have anywhere from fewer than 10 elements to thousands of antennas, so 3000 beams is satisfactory. A hundred delays, however, are in general not enough. Often several hundred or a thousand delays are required. With an increase in the number of bounces to 50, for example, the number of delays can be increased with the quadratic cell to 649 delays. The loss, however, is prohibitive with current liquid-crystal-based SLMs. We predicted and measured losses over 1 dB/bounce, which is almost entirely due to material losses in the SLM and the PBS. Better beam splitters can certainly be obtained, but the loss of the SLM is not expected to improve significantly. A better approach would be to replace the liquid-crystal SLM with a MEM micromirror device, which also removes the need for the beam splitter. The problem of loss reduction is then shifted from the liquid-crystal SLM community to the MEM community, which is optimistic about its ability to comply. A target of 0.1 dB/bounce of MEM loss would allow 60 bounces, or 929 different delays with approximately 10 dB of total loss. If 3 dB for fiber coupling are allowed, then with the remaining 7 dB of a 10-dB loss budget, there could be 42 bounces or 461 delays.

We also found a high level of cross talk, which arose from imperfect extinction of the two polarizations. In one liquid-crystal state, the extinction was excellent, but not in the other. This could be improved with a different design of liquid crystal, but a SLM not based on polarization switching would be preferable.

The loss plus the cross-talk issues clearly point to an alternative SLM such as a MEM micromirror array instead of liquid-crystal-based SLMs. One architecture for a quadratic cell with a MEM device is shown in Fig. 10. We assume here a micromirror array in which the mirrors can tilt to one of two stable positions at $\pm\theta$. When the micromirrors are all tipped to $-\theta$, the light circulates in the White cell formed by mirrors A, B, lens 1, and the MEM device. If, on a given bounce, a pixel is tipped to $+\theta$, then light goes to either E or F, depending on whether it is coming from C or B. We will report on MEM-based White cell TTD devices in a future paper.

Although there is a large number of spots in the White cell, alignment is not difficult to achieve, relying as it does on only the placement of the centers of curvature of the four spherical mirrors. We demonstrated that the low-cost spring-type mounts commonly used are not sufficient to maintain this alignment over time, but use of better quality mirror mounts such as are used for interferometry and holography would fix this problem. A fivefold improvement in stability over the spring-type general-purpose mirror mounts would be required to maintain alignment of 20 spots.

The White cell is an attractive architecture because the alignment is simple, and diffraction losses are negligible. A large number of input beams can be handled simultaneously in a compact space. The fact that the delays incurred depending on the difference in length between alternative paths means that long and short delays are equally easy to implement. The paths can be folded for compactness, and the component count is small, making this a potentially inexpensive, reliable, and physically small device. By use of a MEM micromirror chip as the SLM, most of the loss and all the polarization dependence can be eliminated, making this approach competitive.

This research was based on ideas developed jointly with Stuart A. Collins of the Ohio State University. Many thanks to Bradley D. Stone for help with the figures.

References

1. H. Zmuda and E. N. Toughlian, "Photonic aspects of modern radar," in *The Artech House Optoelectronics Library*, B.

Culshaw, A. Rogers, and H. Taylor, eds. (Artech House, Norwood, Mass., 1994).
2. D. D. Curtis and L. M. Sharpe, "True time delay using fiber optic delay lines," in *Proceedings of the IEEE Antennas and Propagation Society International Symposium Digest* (Institute of Electrical and Electronics Engineers, New York, 1990), Vol. 2, pp. 766–769.
3. R. D. Esman, M. Y. Frankel, J. L. Dexter, L. Goldberg, M. G. Parent, D. Stilwell, and D. G. Cooper, "Fiber optic prism true time-delay antenna feed," IEEE Photon. Technol. Lett. **5,** 1347–1349 (1993).
4. A. P. Goutzoulis and D. K. Davies, "Hardware-compressive 2-D fiber optic delay line architecture for time steering of phased-array antennas," Appl. Opt. **29,** 5353–5359 (1990).
5. W. Ng, A. Narayanan, R. R. Hayes, D. Pereschini, and D. Yap, "High-efficiency waveguide-coupled $\lambda=1.3$ μm $In_xGa_{1-x}As$/GaAs MSM detector exhibiting large extinction ratios at *L* and *X* band," IEEE Photon. Technol. Lett. **5,** 514–517 (1993).
6. A. P. Goutzoulis, D. K. Davies, and J. M. Zomp, "Hybrid electronic fiber optic wavelength-multiplexed system for true time-delay steering of phased array antennas," Opt. Eng. **31,** 2312–2322 (1992).
7. P. M. Freitag and S. M. Forrest, "A coherent optically controlled phased array antenna system," IEEE Microwave, Guid. Wave Lett. **3,** 293–295 (1993).
8. L. Eldada, "Laser-fabricated delay lines in GaAs for optically steered phased-array radar," J. Lightwave Technol. **13,** 2034–2039 (1995).
9. D. A. Cohen, Y. Chang, A. G. J. Levi, H. R. Fetterman, and I. L. Newberg, "Optically controlled serially fed phased array sensor," IEEE Photon. Technol. Lett. **8,** 1683–1685 (1996).
10. R. L. Q. Li, X. Fu, and R. Chen, "High packing density 2.5 THz truetime delay lines using spatially multiplexed substrate guided waves in conjunction with volume holograms on a single substrate," J. Lightwave Technol. **15,** 2253–2258 (1997).
11. A. P. Goutzoulis and J. M. Zomp, "Development and field demonstration of an eight-element receive wavelength-multiplexed true-time-delay steering system," Appl. Opt. **36,** 7315–7326 (1997).
12. B. Tsap, Y. Chang, H. R. Fetterman, A. F. J. Levi, D. A. Cohen, and I. Newberg, "Phased-array optically controlled receiver using a serial feed," IEEE Photon. Technol. Lett. **10,** 267–269 (1998).
13. D. T. K. Tong and M. C. Wu, "Transmit-receive module of multiwavelength optically controlled phased-array antennas," IEEE Photon. Technol. Lett. **10,** 1018–1019 (1998).
14. H. Zmuda, E. N. Toughlian, P. Payson, and H. W. Klumpke III, "A photonic implementation of a wide-band nulling system for phased arrays," IEEE Photon. Technol. Lett. **10,** 725–727 (1998).
15. P. J. Matthews, M. Y. Frankel, and R. D. Esman, "A wide-band fiber-optic true time-steered array receiver capable of multiple independent simultaneous beams," IEEE Photon. Technol. Lett. **10,** 722–724 (1998).
16. R. Taylor and S. Forrest, "Steering of an optically-driven true-time delay phased-array antenna based on a broad-band coherent WDM architecture," IEEE Photon. Technol. Lett. **10,** 144–146 (1998).
17. M. Y. Frankel and R. D. Esman, "Dynamic null steering in an ultrawideband time-steered array antenna," Appl. Opt. **37,** 5488–5494 (1998).
18. D. Dolfi, F. Michel-Gabriel, S. Bann, and J. P. Huignard, "Two-dimensional optical architectures for time-delay beam forming in a phased-array antenna," Opt. Lett. **16,** 255–257, (1991).
19. H. R. Fetterman, Y. Chang, D. C. Scott, S. R. Forrest, F. M. Espiau, M. Wu, D. V. Plant, J. R. Kelly, A. Mather, W. H. Steier, and G. J. Simonis, "Optically controlled phased array radar receiver using SLM switched real time delays," IEEE Microwave Guid. Wave Lett. **5,** 414–416 (1995).
20. X. S. Yao and L. Maleki, "A novel 2-D programmable photonic time-delay device for millimeter-wave signal processing applications," IEEE Photon. Technol. Lett. **6,** 1463–1465 (1994).
21. N. Madamopoulos and N. Riza, "Directly modulated semiconductor-laser-fed photonic delay line with ferroelectric liquid crystals," Appl. Opt. **37,** 1407–1416 (1998).
22. J. White, "Long optical paths of large aperture," J. Opt. Soc. Am. **32,** 285–288 (1942).
23. B. L. Anderson, J. Stuart, A. Collins, C. A. Klein, E. A. Beecher, and S. B. Brown, "Optically produced true-time delays for phased antenna arrays," Appl. Opt. **36,** 8493–8503 (1997).
24. J. U. White, "Very long optical paths in air," J. Opt. Soc. Am. **66,** 411–416 (1976).